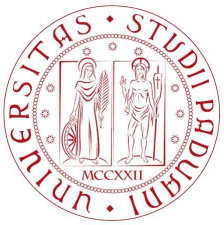

Universitá degli Studi di Padova

Dipartimento di Ingegneria dell'Informazione

Corso di Laurea Triennale in Ingegneria Biomedica

Tesi di Laurea Triennale

Extraction of topological features for the segmentation of endothelial cells in corneal images

Relatore
prof. Alfredo Ruggeri

Correlatore
dott. Enea Poletti

Laureando
Michael Benazzato

Anno Accademico 2012/2013

Abstract

The purpose of this work is to experiment the functionality of customized matched filters to detect the cells' borders in corneal endothelium images. The corneal endothelium is a single thin layer of cells positioned all close together. It maintains the cornea in a dehydrated state, in order to obtain optical transparency. Most of the diseases to the cornea are due to a malfunctioning of the endothelium, and studies have evidenced the correlation between the variation of some morphological characteristics of the endothelial cells and the diseases, principally the cells' shape and the distribution of the areas. The filtering operations have been performed on a set of 30 images with the purpose of detecting those zones of the images that are part of cellular borders. After the filtering operation follows a step of binary classifications of each image's gray levels with different thresholds to evidence which zones are part of features detected and which are not; a comparison with an ideal image to make a ROC curve to evaluate the best classification and then an evaluation of the threshold to apply on a generic application of this method where ideal images are unavailable to make comparisons. All the elaborations on the images and the following analysis have been performed using MATLAB® software.

List of Tables

List of Figures

Contents

Chapter 1

The corneal endothelium

1.1 The cornea

The cornea is a transparent dome-shaped membrane located on the front part of the eye, covering the anterior chamber, the pupil and the iris. The radius of curvature of the cornea is smaller than the eye so it protrudes anteriorly. With the sclera, it forms the *fibrous tunic*, which is the first and the most external of the three tunics that cover the bulb of the eye. Sclera and cornea are connected together in a region called *limbus*, where the cornea is wedge in, like a watch glass.

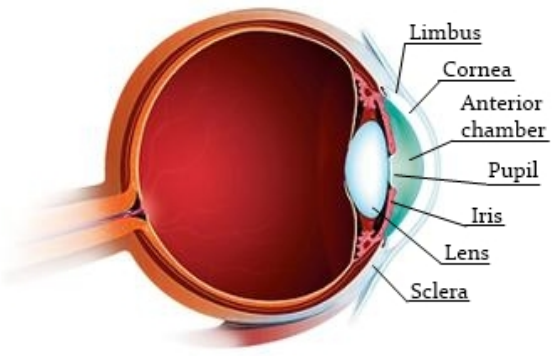

FIGURE 1.1: Cut-away view of the eye.

The cornea is the most sensitive tissue of the body: the density of pain receptor is 300-600 times greater than skin and about 20-60 times greater than dental pulp. So, an injury to the cornea would be extremely painful. A stimulation of the cornea causes an involuntary closing of the eyelid in less than 0.1 seconds. This is called *corneal reflex* or *blink reflex*, and its evolutionary purpose is to protect the eye from foreign bodies.

In addition to its function of eye's protection, the cornea is the first and the most powerful element of the eye's focusing system, accounting the two-third of the total optical power of the eye. The curvature of the cornea gives its focusing power; in the infancy it's spherical and it changes with the age but, unlike the lens, it's not deformable to adjust the focus; so its focusing power is steady.

A vertical section of the cornea shows five layers that globally compose the tissue. From outside to inside:

Epithelium (1): it covers the front of the cornea and it's a barrier that protects the lower layers from the flow of the tears and bacteria.

Bowman's membrane (2): it's a thin layer composed of collagen fibrils and its function is to give and maintain the shape of the cornea.

Stroma (3): it consists of 200 layers of flattened plates of type I collagen fibrils called *lamellae*. In each layer the direction of the collagen fibers is different, to provide maximum mechanical strength.

Descemet's membrane (4): a basement membrane of type IV collagen secreted by the endothelium, located below. It's thin in infancy and increases in thickness in adulthood.

Endothelium (5): the last layer, facing the anterior chamber.

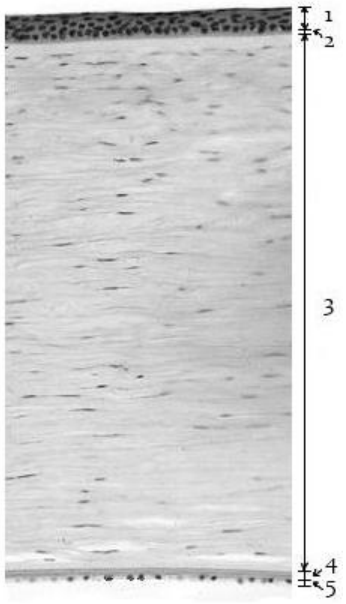

FIGURE 1.2: Microscope image of the corneal layers.

The stroma forms the 90% of the entire thickness of the cornea, that is about 520 μm thick (the other layers cover about the the 10%).

1.2 The endothelium

1.2.1 Anatomy and physiology

The endothelium is composed of a single layer of flattened cells with a predominant hexagonal shape, with a honeycomb arrangement. Given cells of the same area, this disposition is the most efficient, in terms of total

perimeter, to cover the entire posterior surface of the cornea (see Figure 1.3).

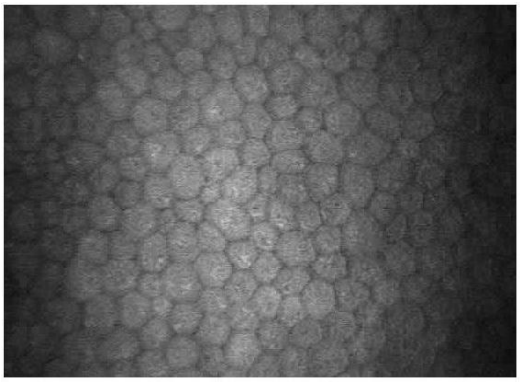

FIGURE 1.3: Microscope image of the corneal endothelium.

Phisiologically, the corneal endothelium is the most important corneal layer. The cornea has to be perfectly transparent to allow an optimal vision. To this purpose, there are no blood vessels: nourishments are provided anteriorly by tears and posteriorly by the aqueous humour. But the transparency of the cornea is mainly due to the collagen fibrils' arrangement in the stroma and in the Bowman's membrane. The corneal layers are mainly composed of collagen, and collagen in human body is usually opaque. But the disposition of the collagen fibrils forms a sort of 3-dimensional array of diffraction gratings, allowing to eliminate by destructive interference the light in all directions except the front. The lamellae in the stroma have to be separated each other less than half a wavelength of light to remain optically transparent.

An excessive hydration causes an incorrect separation between lamellae in the stroma. This disease is called *corneal edema*, and it produces an opacization of the cornea with bad vision consequences. The corneal endothelium, facing the anterior chamber of the eye, is a barrier that carries fluids and solutes from and to the aqueous humour, so it has a fundamental role to maintain the proper state of hydration of the layers above, to guarantee the cornea's transparency, and to provide the necessary nourishments.

1.2.2 Morphological and numerical analysis

Due to his fundamental role for the corneal transparency, many corneal diseases have origin from an incorrect operation of the endothelium. Historically, studies regarding the corneal endothelium had become essential after some surgical operations like the cataract removal. In spite of operations perfectly performed, in the post-operative cloudy and edematous corneas had

been observed, without an apparent logical reason. Afterwards it has been verified that the inauspicious post-operative course was due to an (involuntary) damage to the corneal endothelium.

One of the principal investigations methods is the *corneal endothelial specular microscopy*. It's a non-invasive method used to view and record images of the corneal endothelial cell layer.

FIGURE 1.4: A specular microscope (©Tomey Corp).

Some parameters of clinical interest, indices of the health condition of the endothelium, are:

- *cell density*: the number of cells per mm^2.
- *coefficient of variability (CV)*: it's determined with the equation

$$CV = \frac{SD_{\text{cells' area}}}{\text{mean cells' area}}$$

  with *SD* as standard deviation of the mean cell area, this expressed in $\mu\mathrm{m}^2$.

- *hexagonality coefficient (HEX)*: percentage of the six-sided cells.

The post-natal amount of total cells that composes the endothelium is achieved by the sixth week of gestation, and it's about 390000 to 560000 cells per cornea. Till to the first few years of life the number of cells remain the same, but the spatial density decreases rapidly due to the cornea growing, regardless of the presence of diseases to the tissue. In the adulthood there are no sensible variations to the cornea's dimension, but the density of cells decreases anyway in a linear manner and more slowly (about 0.6 % per year): this indicates that the physiological cell death due to tissue ageing is not balanced by regeneration. Hence, the human corneal endothelial cells has a

very limited capability to proliferate in vivo. When the corneal endothelium is damaged, the healing process doesn't carry out with mitosis, but with a process of enlargement of the cells, to fill the holes left by the died ones.

The degree of cellular loss due to diseases, trauma, chemical toxicity or other causes can be observed with specular microscopy as a decrease of the cell density (less cells per unit area), an increase in the variation of the individual cells area and a change of the cells' shape. Studies have shown that the function of the endothelium is compromised when the cells' density decreased under the threshold of 500 to 1000 cells per mm^2.

The variation in cell area is called *polymegethism*, and the CV is its indicator. A normal value of CV and then of polymegethism is about 0.32 (32%). The variation in cell shapes is called *pleomorphism*, and HEX is its indicator. Polymegethism and pleomorphism are correlated; a changing in cells' area due to a surface expansion implies a changing in cells' shape.

1.3 Treatment for the diseases

Due to the natural limited (if not absent) capability of the endothelial cells to proliferate in vivo, there are no medical solutions to stimulate the proliferation, both in case of disease or injuries. The unique solution in these cases is the corneal transplantation.

The corneal transplantation requires a donor cornea and usually the prognosis is very good. The healing time is slower than other body parts due to the lack of blood vessels, but for the same reason risks of rejection are very low.

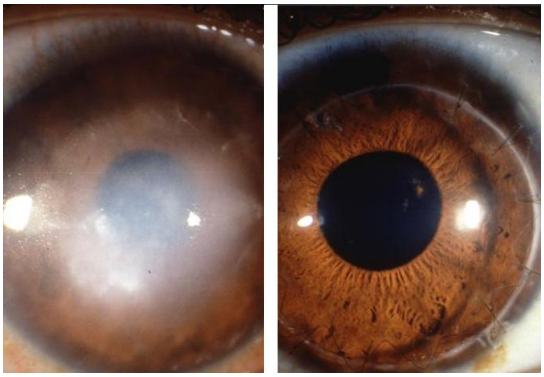

FIGURE 1.5: A human eye with edematous cornea before the corneal transplant (on the left) and after the transplant (on the right).

As any other transplant operation, the possibility to perform it it's related to the number of cornea donors, that are not frequent as would be necessary:

the cornea donor has to be possibly young (in order to avoid future diseaes to the receiving due to tissue ageing) and in good health state. Also, in case of failure of the transplantation, a second operation would have a significant worse prognosis than the previous one.

An alternative to the corneal transplant is to use the tissue engineering to reproduce in vitro the endothelial layer cultivating endothelial cells. Despite its capacity to proliferate in vivo, it has been demonstrated that the endothelial cells have capacity to proliferate in vitro. The idea have been conceived over three decades ago and it's still subject of researches in order to find the best technique to isolate the endothelial cells and to create a good carrier in which to grow the cells.

Chapter 2

Corneal endothelium images' segmentation

2.1 Mathematical briefings

An image can be generally represented with a two-dimensional function

$$f : [a, b] \times [c, d] \subset \mathbb{R}^2 \to \mathbb{R}^n \qquad z = f(x, y) \tag{2.1}$$

The domain $[a, b] \times [c, d] \subset \mathbb{R}^2$ represents a rectangular plane whose dimensions equals the image's ones. The spatial coordinates (x, y) represent a point in the plane of the image, with the origin at the top corner left, the z-axis outgoing perpendicularly from the plane and the x-y axes placed along the borders of the image following to the right hand rule (see Figure 2.1).

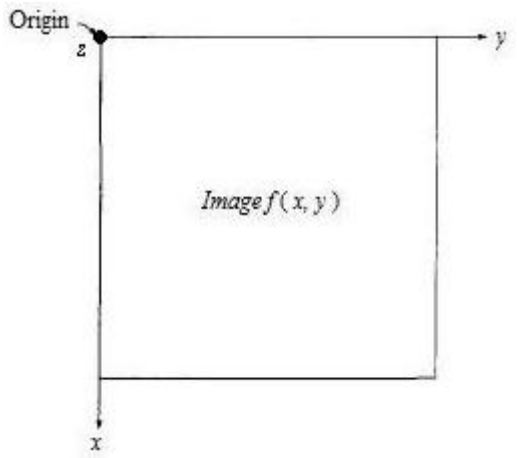

FIGURE 2.1: The standard reference system on an image.

A value $z_0 = f(x_0, y_0)$ is the amplitude of the function on the point (x_0, y_0). If the image is gray-scaled, the amplitude z_0 is a real number ($n = 1$ in formula 2.1) in a real interval whose a minimum value corresponds to black and whose maximum value corresponds to white. If the image is coloured, the value of z is a vector of usually three components ($n = 3$ in formula 2.1), each for red, green and blue levels that together give the color in that point.

On this work all gray-scaled images have been used.

If the x, y and z are all discrete quantities, the image is a *digital image*. In this case:

$$f : [a, b] \times [c, d] \subset \mathbb{Z}^2 \to \mathbb{Z}^n \qquad z = f(x, y) \tag{2.2}$$

A digital image can be imagined like a grid in which every square is identified by a couple (x_p, y_p) and it's called *pixel*, short for *picture element*.

A mathematical representation of a digital image that is more suitable for most applications consists on using, to represent the image, a matrix whose dimensions corresponds to the image ones. Each element of the matrix represents a pixel and the number in it is the corresponding gray level.

2.2 Image filtering in the spatial domain

The objective of image enhancement is to make an image more suitable for application purposes. For example in medical field the image enhancement can allow a better diagnosis by equalization, filtering, contrast or brightness adjustment and other elaborations.

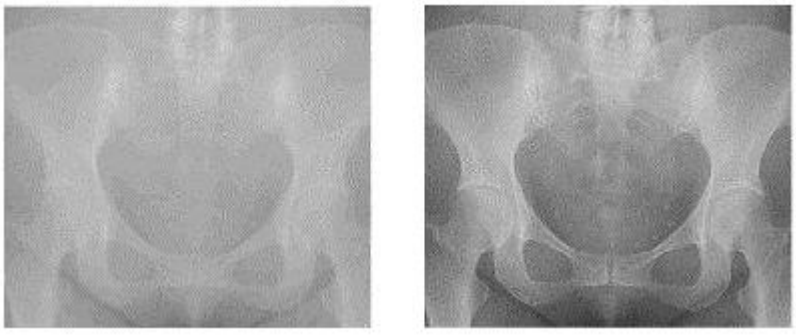

FIGURE 2.2: An example of image enhancement to improve its definition. On the left, the original x-ray image of the pelvis; on the right the image resulting from the elaboration.

The image enhancement can be executed in the *spatial domain* or in the *frequency domain*. The term *spatial domain* indicates that the elaborations to enhance the image take place on the plane of the image, acting directly on

its pixels. In the *frequency domain* the enhancements are made considering the Fourier transform of the image. In both cases, the main goal is to improve the information content of the image.

The enhancement of the image in the spatial domain consists on evaluating, pixel by pixel of the image, a neighbourhood of a pixel with a subimage wide as the neighbourhood. The subimage used to filter the original one is called *filter*, *kernel* or *mask*. In some cases the kernel is used to change the value of the central pixel: an example could be a mask used to substitute the value of a pixel with the average value of the pixels in the neighbourhood (this mask is called *average filter*). In other cases the kernel is used to verify if the image has some properties in the area covered by the neighbourhood.

The corneal endothelium images have been processed with the second technique: filters have been used to verify the presence of some features on them. These filters take the name of *matched filters*, because they are used to find a "match" between the portion of image examined by the filter and an object represented by the filter (a segment, an edge, etc).

Given a $M \times N$ image represented by the function $f(x, y)$ and a $m \times n$ mask $w(s, t)$, the *response* of the linear filtering process of the image with the mask is given by the summation of the multiplication of each pixel of the filter with its correspondent on the image:

$$R = \sum_{i=-a}^{a} \sum_{j=-b}^{b} w(i, j) f(x + i, y + j)$$

where $a = (m-1)/2$ and $b = (n-1)/2$ and (x, y) are the coordinates of the pixels on the image. To filter the whole image, it has to be $x = 0, 1, ..., M-1$ and $y = 0, 1, ..., N-1$.

With this technique the filter "moves" on the image in a sort of scan and applies the filter on a portion of the image wide as the dimensions of the filter, and recognize the presence of features in that area. The filter's coefficients $w(i, j)$ "weight" each pixel of the image in order to emphasize those one that are part of the feature to detect. Then, the filter response will be higher where features are present and lower in the other parts. From this elaboration will results an image with brighter areas where the algorithm has detected features the rest will be darker.

In this way, a problem take place near the borders of the image. When the distance from the filter's center and the image border is less than half each filter dimension, the filter protrudes out from the image plane. To obtain a resulting image with the same dimensions of the original one, it's then necessary to enlarge the image in order to allow the filtering of the zones near the image borders. This operation is known as *image padding*:

the pixels that are part of the enlarged portion have usually zero value or replicates (specularly) the rows and columns of the image. The filtering can be then performed, and the padded region it's removed at the end of the operation.

2.3 Segmentation of the corneal endothelium images

To recognize the cells on the corneal endothelium images three types of filters have been used, each for a particular feature: the cells' sides, the cells' centers and the cells' trifurcations.

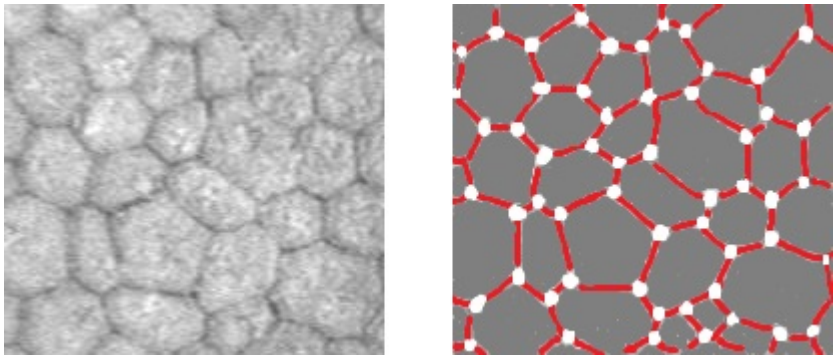

FIGURE 2.3: On the left, a portion of corneal endothelium image; on the right the same image where cells' edges (red), trifurcations (white) and centers (gray) have been emphasized.

The three filters recognize different features in the images with the ultimate goal of producing an image where the cellular contours are highlighted. The choice of using three different filters has been made to improve the precision of the segmentation, in order to made a better selection of the pixels of the original image. For example, a pixel that in the original image is part of a cellular contour has more probability to be detected correctly if there are more than one filter that operates on it. In particular, the filters detecting the edges and the trifurcations allow to define which pixels belong, on the image, to a cellular edge and the filters to detect the cellular centers allow to detect which pixels on the image do *not* belong to a cellular edge.

2.3.1 Detection of the cells' edges

The endothelial cells have mainly a polygonal shape, so to detect the cells' edges it's necessary to use a filter able to detect a sort of segment, that

in the original image corresponds to a side of a cell. The matched filter used to recognize the cells' edges has been realized with a square matrix of all zero values except for lines of all ones. When the filter is applied to the image, the matching is obtained if a side of a cell on the original image overlies the lines of all ones in the filter. Here are two examples of a 5-by-5 matrix that realizes such a filter:

$$\begin{bmatrix} 0 & 0 & 0 & 0 & 0 \\ 1 & 1 & 1 & 1 & 1 \\ 1 & 1 & 1 & 1 & 1 \\ 1 & 1 & 1 & 1 & 1 \\ 0 & 0 & 0 & 0 & 0 \end{bmatrix} \qquad \begin{bmatrix} 0 & 0 & 0 & 1 & 1 \\ 0 & 0 & 1 & 1 & 1 \\ 0 & 1 & 1 & 1 & 0 \\ 1 & 1 & 1 & 0 & 0 \\ 1 & 1 & 0 & 0 & 0 \end{bmatrix}$$

The matrix on the left represent a filter able to detect a horizontal edge, the matrix on the right is able to detect an edge rotated of $\frac{\pi}{4}$ radians.

Putting the filter on a $x - y$ reference, the filter is centered on (0,0), that is the central element (on the examples above, the element on the third row and third column) has coordinates (0,0). The $x - y$ are oriented as shown in Figure 2.1. The filter's dimension have to be an odd number, in order to have ever a central element.

To adapt the filter to the various cells' edges orientations, the filter is rotated in steps of $\frac{\pi}{12}$ radians around the central element for 12 times, covering uniformly a turn. During the filtering, each rotated version of the filter is applied on the same area in order to find the best correspondence. This is identified by the higher filter response among all the rotated versions.

In Figure 2.4 below are shown a portion of the original image of the endothelial cells and the same portion after the application of a 9-by-9 filter:

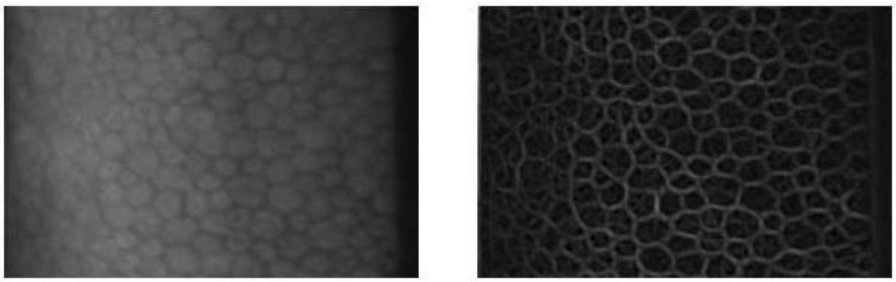

FIGURE 2.4: On the left, a portion of corneal endothelium image; on the right the same image after the application of the filter.

In the filtered image can be noted some brighter segment on areas that in the original image are cells' centers. This point out the presence of noise

in the original image that the filter doesn't eliminate; but in the analysis of the results will be described the irrelevance of this factor.

2.3.2 Detection of the cells' trifurcation

A *trifurcation* is formed by three cells' sides with an end in common. The matched filter used to recognize the cells' trifurcation has been realized merging four gaussian functions in the 3-D space in order to reproduce the shape of the real trifurcations present on the images. A 3-D plot of the resulting filter is shown on Figure 2.5.

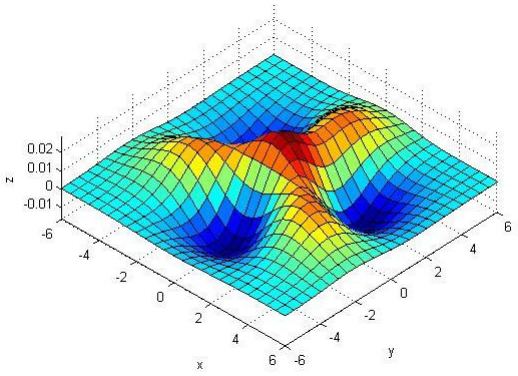

FIGURE 2.5: A 3D representation of the filter to detect the trifurcations.

The plane of the filter is divided by the arms of the trifurcation into three equal parts of $\frac{2}{3}\pi$ radians each.

A gaussian function in the 3-D space is defined by the formula:

$$g(x,y) = Ae^{-\left(\frac{(x-x_0)^2}{2\sigma_x^2}+\frac{(y-y_0)^2}{2\sigma_y^2}\right)}$$

where A is the amplitude, (x_0, y_0) are the coordinates in which the gaussian is centered to and σ_x, σ_y express the x and y spreads of the lob. In the algorithm used, the lob is symmetric on both $x-y$ directions, so $\sigma_x = \sigma_y = \sigma$, and the formula used is

$$g(x,y) = Ae^{\frac{(x-x_0)^2+(y-y_0)^2}{2\sigma^2}}$$

The first gaussian function $g(x,y)$ realizes the central peak, corresponding to the center of the trifurcation. It's centered on the center of the filter (so $(x_0, y_0) = (0,0)$).

The other three gaussian function $n_1(x,y), n_2(x,y), n_3(x,y)$ realize the three peaks that protrude under the plane of the filter. Each of these functions has been centered on a point positioned at a distance of $\sqrt{\sigma}$ from the

center of the trifurcation, along the bisector of each of the three plane portions formed by the trifurcation.

Each of these functions, $g(x, y)$ and $n_i(x, y), i = 1, 2, 3$ have been realized on a $x - y$ square grid that represents the plane of the filter. Each element in the grid represents a point (x, y) of the plane. The values on each of these functions are memorized on a square matrix of the same dimension of the grid: the matrix F which contains the values of the final filter shown in Figure 2.5 is obtained summing the four matrices of the functions values:

$$F = A \cdot g(x, y) - [n_i(x, y)] \qquad i = 1, 2, 3$$

with the parameter A that can be adjusted to regulate the amplitude of the peak at the center of the trifurcation.

The filter has been realized in various scales, to adapt it to the various dimensions of the trifurcations on the original endothelial image. The scale has been varied acting on the value of σ, so on the spreads of the four lobs. In the image processing, this parameter σ is known as the *scale-space parameter*, because it defines how fine is the filter action. Also, for each scale the filter has been realized in eighteen rotated version around the central z axis. The step of rotation is $1/18$ of $\frac{2}{3}\pi$, to cover uniformly an entire turn.

Figure 2.6 below shows a portion of the original image of the endothelial cells and the same portion after the application of a 13-by-13 pixels filter with an amplitude $A = 2$ of the central gaussian function.

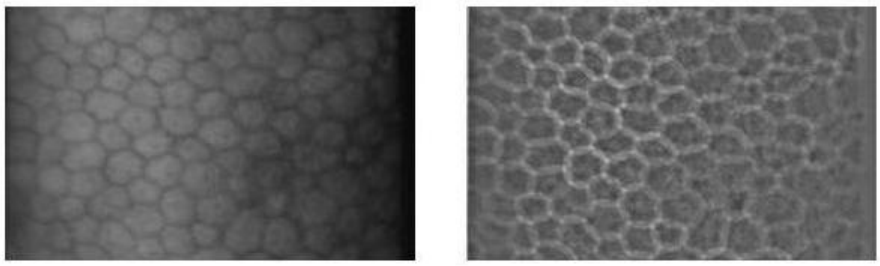

FIGURE 2.6: On the left, a portion of corneal endothelium image; on the right the same image after the application of the filter.

It can be noted, especially in the left part of the filtered image where the definition in the original one is more clear, that the center of the trifurcations are evidenced approximately with a white dot. This is important because on the analysis of the filter, described up ahead, the filtered image will be compared with an ideal image result where the trifurcations are highlighted as small dots in correspondence of the each trifurcation center.

2.3.3 Detection of the cells' centers

The cells' centers can be detected using a very common filter called *Laplacian of the Gaussian* (*LoG*) because it's based on the operator of the same name. The resulting filter has this shape:

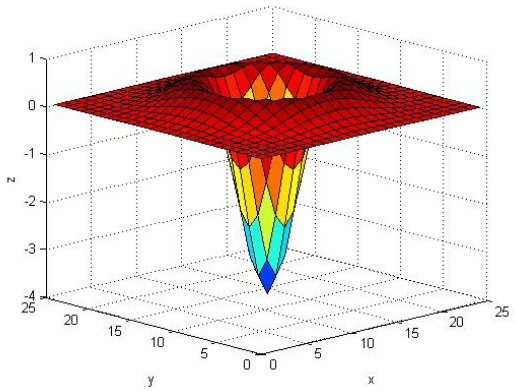

FIGURE 2.7: A 3D representation of the LoG filter to detect the cells' centers.

The LoG filter first convolves the image $f(x, y)$ with a gaussian filter $g(x, y)$:

$$F(x, y) = f(x, y) * g(x, y)$$

then, the Laplacian operator is applied to the convolution result, to obtain the filtered image L:

$$L(x, y) = \nabla^2 F(x, y) = \frac{\partial^2 F}{\partial x^2} + \frac{\partial^2 F}{\partial y^2}$$

In the discrete version, the equation above becomes:

$$\frac{\partial^2 F}{\partial x^2} = F(x+1, y) + F(x-1, y) - 2F(x, y)$$
$$\frac{\partial^2 F}{\partial y^2} = F(x, y+1) + F(x, y-1) - 2F(x, y)$$

and then

$$\nabla^2 F(x, y) = [F(x+1, y) + F(x-1, y) + F(x, y+1) + F(x, y-1) - 4F(x, y)]$$

The LoG filter is generated automatically with a specific MATLAB® function. Also in this case, it's necessary to implement the filter with various scales due to the various areas of the cellular centers on the endothelial images, in order to find the best correspondence at ever filtering operation. The scales are changed acting on the spread of the lob that protrudes under the plane of the image.

The results of the application of the filter are shown in Figure 2.8, compared to the original image. The filter implemented is 35-by-35 pixels with four different scales of 3, 3.5, 4, 5.

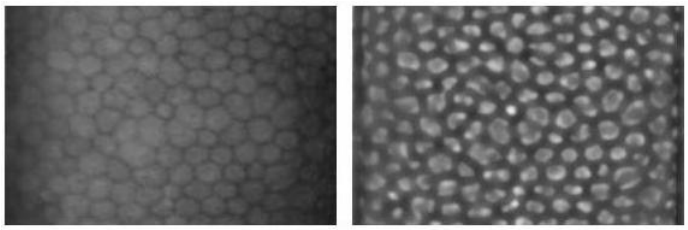

FIGURE 2.8: On the left, a portion of corneal endothelium image; on the right the same image after the application of the filter.

Chapter 3

Classifications ad evaluations on the filtered images

The procedure of classification on the filtered images is the second part of this work, and its purpose is to establish which pixels of the image are part of the features detected and which are not. After the classification a quantitative analysis on how many pixels have been correctly detected as part of features and how many have not been detected is necessary, to have a first evaluation of the performance of the classification.

3.1 The problem of classification

3.1.1 Binary classification

The term *classification* indicates the assignation procedure of an instance to a particular group, depending on the characteristics of the instance itself. A generic *classifier* makes a classification mapping a set X of instances in another set Y of *labels*. To every instance is assigned a label if the instance has some properties, verified by the classifier. The classifier is *binary* if the labels that can be assigned to every instance are only two.

A very common example of binary classifier is every medical test that, analysing human biological samples, provides an indication of the patient's health state. In these cases, the set of instance consists on the patients to be tested, and the two labels are usually named *positive* or *negative* to indicate respectively an *abnormal* or a *normal* state.

The classifier marks an instance with one of the two labels usually depending on a value of a parameter related to the instance itself. The classifier use a threshold value called *cut-off value*: the instances with a parameter value

above the cut-off value are marked with a label, the other ones with the other label. In the example of the medical test, the two categories in which each patient can result into depends on a concentration of substance present on the biological sample. A concentration above a cut-off value indicates that the patient is diseased, in the other case it's in health. More often there are two different cut-off values, in order to say that the patients with concentration between the two values are in health and in the other cases are diseased. In every case, the classification is binary.

Denoting with x_i as a generic element of the input set X of instances given to the classifier, with p_{x_i} the parameter related to the instance x_i and with t_h the cut-off value, the action of a binary classifier can be summarized with the sequent definition:

$$\forall x_i \in X, \qquad \begin{cases} x_i \rightarrow \text{positive} & \text{if } p_{x_i} \geq t_h \\ x_i \rightarrow \text{negative} & \text{if } p_{x_i} < t_h \end{cases}$$

3.1.2 Performance of a binary classifier

It's necessary to distinguish from the label given by the classifier and the actual state of the instance classified. The classifier acts depending on only the setted cut-off value; that is, the assignment of the label positive or negative by the classifier to an instance is a *prediction* of the instance's actual state; so the classifier states that the instance has *a probability* to be actually positive or negative.

In the medical example, the result of a clinical test indicates the health state of a patient with a certain probability, and sometimes other exams are necessary to assure that the result of the first test corresponds to the real condition of the patient.

Performing the classification of a set X of instances, both the positive and negative labeled instances tend to distribute normally around the mean parameter value that characterise each of the two groups. If, ideally, the two distributions would be separated, it would be possible to give to the classifier a cut-off value able to detect correctly all the instances: that is to say that the instances that are actually positive are classified as positive, and the instances that are classified as negative are actually negative (Figure 3.1a).

But always happens that the two distributions overlap themselves: in this case there is not a cut-off value that makes the classifier able to separate absolutely the two categories of instances (Figure 3.1b). This implies that there will be instances classified as positive that really are negative, instances classified as negative that are really positive and instances correctly classified.

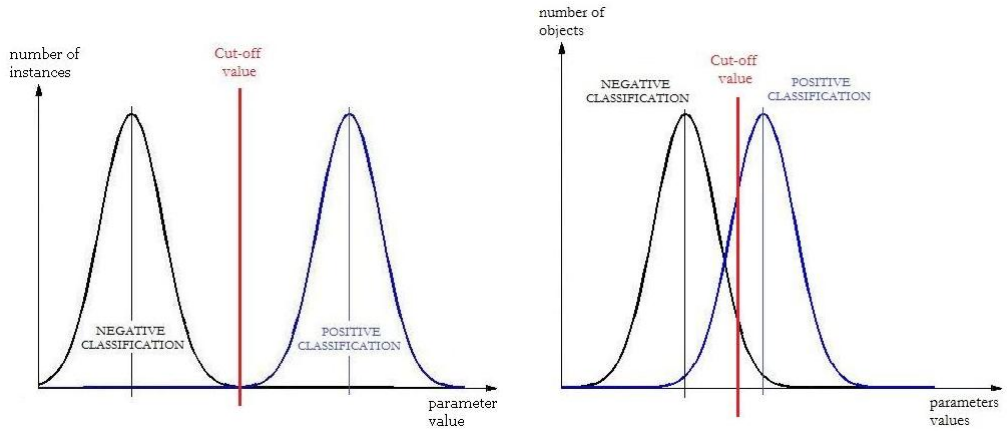

(A) an ideal wide separation between the distributions allow to determinate an absolute cut-off value.

(B) the overlap of the distributions doesn't allow to determine an absolute cut-off value.

FIGURE 3.1: Examples of distributions of the instances.

In Figure 3.1b, assuming that an instance with parameter greater or equal the cut-off value is labeled as positive and the other negative, the area under the curve of the negative classification at the right of the cut-off value is the number of instances labeled as positive but that they are really negative; similarly the area under the curve of the positive classification that is at the left of the cut-off value constitutes the number of instances labeled as negative but they are really positive.

So every instance classified, compared with his real state can constitute one of the four sequent cases:

- **true positive (TP)**: the instances in input of the classifier that are really positive and the classifier marks as positive;
- **false positive (FP)**: the instances in input of the classifier that are really negative and the classifier marks as positive;
- **true negative (TN)**: the instances in input of the classifier that are really negative and the classifier marks as negative;
- **false negative (FN)**: the instances in input of the classifier that are really positive and the classifier marks as negative.

These results can be summarized on a *contingency table*:

Obtained the number of *TP, FP, TN, FN* it's possible to calculate some parameters that indicate the performances of the classifier:

TABLE 3.1: *Contingency table* of binary classification results.

		Real value	
		P	*N*
Classifier response	*P*	**TP**	**FP**
	N	**FN**	**TN**

1. ***true positive rate (tpr)***: it's the ratio between the TP detected by the classifier and all the really positive instances:
$$tpr = \frac{TP}{TP + FN}$$
It express the *hit rate*, the percentage positives that have been correctly classified. It's also called ***sensitivity***.

2. ***false positive rate (fpr)***: it's the ratio between the FP detected and all the really negative instances:
$$fpr = \frac{FP}{FP + TN}$$
It express the *false alarm rate*, the percentage of real negatives instances that the classifier has wrongly detected positive.

3. ***specificity***: it's the ratio between the TN detected by the classifier and all the really negative instances:
$$specificity = \frac{TN}{FP + TN} = 1 - fpr$$
It's also called *true negative rate*, because it express the percentage of negatives that have been correctly classified.

4. ***accuracy***: it's the ratio between all the instances correctly classified (TP and TN) among all the instances:
$$accuracy = \frac{TP + TN}{TP + TN + FP + FN}$$

3.2 Classification and comparison of the filtered images

A procedure of (binary) classification can be performed on the corneal endothelium filtered images in order to evaluate the performance of the filters used.

The classification procedure wants to mark as *positive* those pixels that are part of the features detected, and mark as *negative* those pixels that are not part of the featured detected. As the filtered images have the features detected brighter and the other zones darker (see Figure 2.4, 2.6, 2.8) the pixels that are positive or negative will results respectively white or black after the classification.

The decision to make a pixel white (positive) or black (negative) is made setting a *cut-off* value on the gray levels of the filtered images. The gray scale of the filtered images is normalized, to have gray levels between 0 (black) and 1 (white). Setting a cut-off value for the gray levels from 0 to 1, pixels that have a gray level greater than the cut-off value will result white, the others will result black.

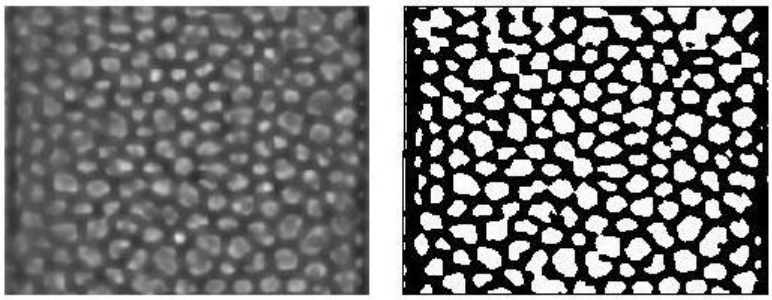

FIGURE 3.2: An example of classification of a filtered image to detect the cells' centers. On the left, the filtered image; on the right, the image after the pixels' classification.

As listed on the previous section, the classification gives a prediction of the real state of the instances in input: similarly, the classified image constitutes a prediction of the zones where the filter have detected the presence of features (in white) and not (in black). It's necessary to verify the correctness of these predictions comparing the image resulting from the classification with an ideal image that contains the correct information about the zones where there are features or not. This image has been hand-made from the original one. An example is shown in Figure 3.3.

The hand-made images reproduce only a portion of the total cells present in the original one. This is due to the quality of the original images, which present bright zones, darker zones, zones with a better definition and other blurred ones. The classification has meaning if it's performed on those zones of the images where it's possible achieve correct informations about the presence of features that have to be detected. The blurred or too dark zones of the images are then excluded from the classification because in them no certain information can be achieved. The region of the image that is object of analysis is called *region of interest*.

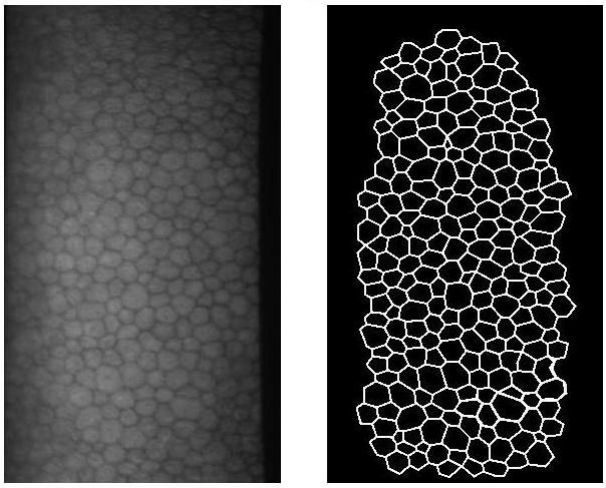

FIGURE 3.3: On the left, the original image; on the right, the hand-made image of the cellular borders.

To perform this, it's necessary to extract from each hand-made image the pixels that constitutes the features that the filter have to detect: for example, for the filtered images to detect the trifurcations it's necessary to have an image in which are shown the real points where the trifurcations are present, to make a correct comparison. The same for the other two types of filters. The image resulting from the extraction of the features from the hand-made one is called *ground truth*.

With the image classified and the *ground truth* can be performed a comparison to evaluate the number of true positive, false positive, true negative, false negative:

- A **true positive** is each pixel that in both the classified image and the ground truth is part of a feature (white);
- A **false positive** is each pixel that in the classified image results part of a feature (white) but it's not in the ground truth (black);
- A **true negative** is each pixel that in both the classified image and the ground truth is not part of a feature (black);
- A **false negative** is each pixel that in the classified image doesn't result part of a feature (black) but it's so in the ground truth (white).

An example of comparison in shown in Figure 3.4.

(A) the image classified;

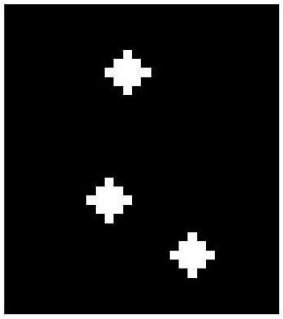

(B) the ground truth;

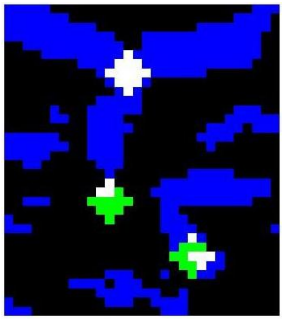

(C) the results of comparison. *TP* are white, *TN* are black, *FP* are blue, *FN* are green.

FIGURE 3.4: An example of comparison between classified image and ground truth.

3.2.1 *Ground truth* for the trifurcations

To obtain the *ground truth* for the trifurcations, the cellular borders of the hand-made image have been reduced in thickness in order to have borders of one pixel thick. Then, for every white pixel (that is a pixel that is part of a border) has been considered a neighbourhood forming a 3-by-3 matrix with the pixel at the center. So, the generic matrix is

$$\begin{bmatrix} a & b & c \\ d & 1 & e \\ f & g & h \end{bmatrix} \tag{3.1}$$

where the central white pixel is signed with a "1".

The square matrix represents a trifurcation in three main cases:

$$\begin{bmatrix} 1 & 0 & 1 \\ 0 & 1 & 0 \\ 0 & 1 & 0 \end{bmatrix} \quad \begin{bmatrix} 1 & 0 & 1 \\ 0 & 1 & 0 \\ 0 & 0 & 1 \end{bmatrix} \quad \begin{bmatrix} 1 & 0 & 0 \\ 0 & 1 & 1 \\ 0 & 1 & 0 \end{bmatrix}$$

for each of these three cases there are other three cases that corresponds to the same matrix but rotated of $k\frac{\pi}{2}$ radians, $k = 1, 2, 3$. No other cases are possible, due to the reduction of the cellular edge's thickness.

The three main cases above, and then the rotated ones, can be automatically detected verifying:

- if there are an adjacency on the corners, where the adjacency is defined as the condition for which the corner is "1" and the two elements adjacent are both "0";

- if there are adjacencies on the other elements that are not corners (the elements *b, d, e, g* in the matrix 3.1.

Referring to the general matrix 3.1, and indicating with "&" the logical AND, with "|" the logical OR and the logical NOT with the overline, these two checks can be realized counting the total number of adjacencies:

$$\begin{aligned} \mathbf{ad1} &= a \;\&\; (\overline{b \mid d}) \\ \mathbf{ad2} &= c \;\&\; (\overline{b \mid e}) \\ \mathbf{ad3} &= f \;\&\; (\overline{d \mid g}) \\ \mathbf{ad4} &= h \;\&\; (\overline{g \mid e}) \end{aligned}$$

$$\mathbf{ad_{tot}} = \mathrm{ad1} + \mathrm{ad2} + \mathrm{ad3} + \mathrm{ad4} + (b + d + e + g)$$

where the first four equations perform the checking of the adjacencies on the corners, and the last one gives the total adjacencies adding the ones of the elements that are not corners.

If the total number ad_{tot} of adjacencies is greater or equal of three, the trifurcation is detected. When this happen, in the *ground truth* image the 3-by-3 matrix is reported in the same position and slightly enlarged in order to reproduce a dot (to "mark" the position in which the trifurcation has been detected). The *ground truth* image consists then of multiple dots in correspondence of where the centers of the trifurcations have been detected.

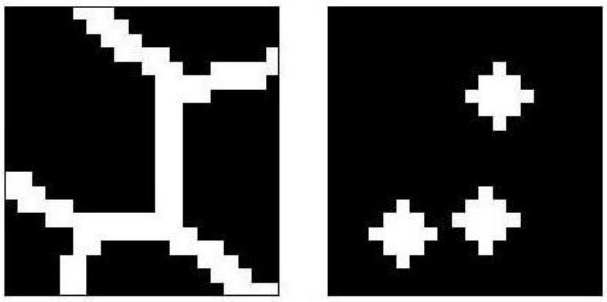

FIGURE 3.5: A crop of the original hand made image (on the left) and the same crop with the trifurcations marked (on the right).

3.2.2 *Ground truth* for the cells' edges

The cells' edges can be evidenced removing the zones where the trifurcations are detected from the original hand-made image.

As in the case of the trifurcations, the borders of the cells in the original hand-made image are reduced to the thickness of one pixel and then is

repeated the algorithm to detect the trifurcations. When a trifurcation is detected, the central pixel and a 5-by-5 neighbourhood are eliminated from the image, leaving the three cells' sides without the center that joined them. The borders in the resulting image are then expanded, giving an image like the one shown in Figure 3.6.

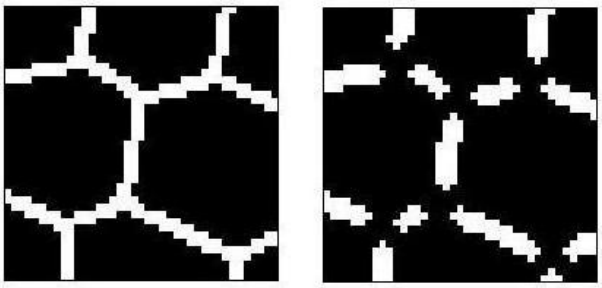

FIGURE 3.6: A crop of the original hand made image (on the left) and the same crop with the edges marked (on the right).

3.2.3 *Ground truth* for the cells' centers

To obtain the *ground truth* for the cells' centers, from the original hand-made image the cells' centers are made white and the thickness of the cellular borders is increased.

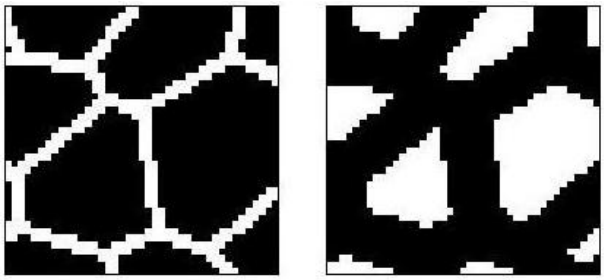

FIGURE 3.7: A crop of the original hand made image (on the left) and the same crop with the centers marked (on the right).

Chapter 4

Analysis of the filters' performances

In Section 3.1.2 has been explained that after a procedure of classification follows a step of evaluations to obtain some parameters that indicate the performance of the classifier (shown on page 27). Referring to Figure 4.1 it's possible to denote that a changing in the cut-off value used to make the classification implies a variation on the number of true positive, true negative, false positive and false negative resulting from that classification; and, a variation of these parameters implies a variation of the specificity, sensitivity and accuracy values. In other words, the cut-off value variation implies the *discriminatory capability* variation of the classifier.

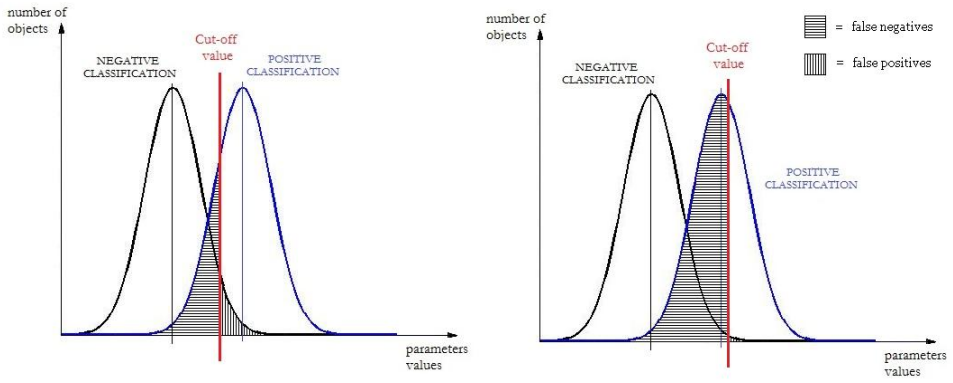

FIGURE 4.1: The two plots show the difference in number of *false positive* and *false negatives* (both fails of the classifier) on varying of the cut-off value.

The higher the cut-off value, the greater the number of true negatives; but there will be an increasing number of false negatives and a lower number of true positives. The lower the cut-off value, the greater the number of true

positives, but there will be an increasing number of false positive and a lower number of true negatives.

Every filtering procedure has been tested on a set of 30 images. This chapter explains the procedure adopted to identify the best threshold value to make the classification of each filtered image. To make this evaluation the ROC curve has been used. Finally, for every of the three filtering operations, the mean of the best threshold has been applied to classify again all the images, in order to evaluate that threshold as the "candidate" best one to apply on a generic application of this method of image filtering, where no ideal image are available to make a comparison with the image resulting from the classification.

4.1 The receiver operating characteristic (ROC)

4.1.1 The ROC curve

The *receiver operating characteristic* or simply called *ROC curve* is a graph that reports the performance of a binary classifier on varying of the cut-off value chosen to make the classification. Each point of the plot reports the values of *specificity* versus *sensitivity* (*true positive rate*) for the correspondent cut-off value. The specificity values are reported on the x axis, the values of sensitivity are reported on the y axis. Because the values of *fpr* and *tpr* are always between 0 and 1, the ROC graph is plotted on a 1-by-1 square plane, also called *ROC space*.

For historical reasons, usually on the x-axis are reported the values of 1 - *specificity* that corresponds to the values of false positive rate *fpr*. The choice to report *specificity* or 1-*specificity* in the x-axis does not change the plot; the two versions are only specular.

On a real classification, due to the finite values of threshold that can be given to a classifier, the ROC curve would be made of a finite number of points; but better descriptions (without information loss) can be obtained by interpolation or by union of consecutive points, obtaining a polygonal (see Figure 4.2).

The *sensitivity* or *true positive rate* expresses the percentage of positives that have been correctly classified; it's an indicator of the *probability* that the classifier detects a positive when the instance examined is actually positive. Instead, the *false positive rate* indicates the percentage of positives that have been incorrectly classified as positive; it's an indicator of the *probability* of false alarm by the classifier (cfr. Section 3.1.2). The ROC curve, that reports this pair of indices for every cut-off value, is a function that connects the two

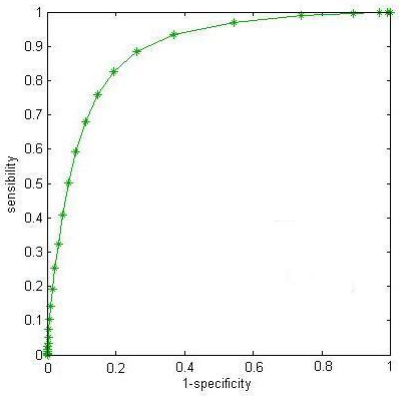

FIGURE 4.2: Example of a polygonal ROC curve obtained by union of consecutive points.

probabilities together on varying of the cut-off values.

4.1.2 Analysis of a ROC graph

The area under the curve

One of the most important parameter to consider on the analysis of a ROC graph is the *area under the curve*, often written with only the acronym AUC. It has been demonstrated that the AUC value establish *the probability that a randomly chosen really positive instance would be ranked higher from the classifier than a randomly chosen negative one*. In other words, the AUC value expresses the percentage of *discriminatory capability* of the classifier. This interpretation of the AUC poses in evidence two characteristics:

- the best classification is the one whose ROC curve pass through the point (1-*specificity*,*sensitivity*) = (0,1). In this case all the positive instances are classified as positive (*sensitivity* = 1) and there are no false positive (all the negative are correctly classified, *specificity* = 1). The AUC value is 1 (100% of probability that a really positive instance would be classified as positive).

- the points in the ROC space that stays in the *minor diagonal* (the diagonal that starts from the lower left corner to the upper right one) corresponds to a random classification. In fact, assuming to have a ROC curve like the described diagonal, the AUC value would be 0.5, and this would imply that the classifier has the 50% of probability to classify correctly a real positive or negative instance, as if the classification would made with a coin toss.

Assuming to approximate the ROC curve with a polygonal, the AUC value can be approximated with the summation of the trapezoid areas. For a classification made with n cut-off values and denoting with Sp_i and Se_i respectively a generic i-th value of specificity and sensitivity, each trapezoid area is given by the formula:

$$A_{tp} = \frac{[\mathrm{Sp}_i - \mathrm{Sp}_{i-1}] \cdot [\mathrm{Se}_i + \mathrm{Se}_{i-1}]}{2} \qquad i = 1, \ldots, n$$

The approximation is better if the number of cut-off values used is high enough.

The meaning of the AUC suggests to divide the ROC space into two regions by the minor diagonal: all the points above this diagonal indicate a performance of classifier better than random; the points under the diagonal indicate a performance worse than random. The usage of the ROC curves in the real situations (such like medical tests or the present work) cannot cause cases in which the classification is worse than random; such a situation would indicate an error on the classification procedure. The expected AUC value is then 0.5, and the deviation from this value is a comparison index to evaluate a better classification of an entire instances set from another (that is, to make a comparison of two different ROC curves for the same instances set).

Research of the best cut-off value

An intuitive criterion to find the best cut-off value among the n adopted for a classification is to find the threshold that constitutes the best compromise between specificity and sensitivity. In a ROC curve the procedure can be performed evaluating the distance of every point of the curve to the point (0,1) in the upper left corner, which represents the best classification. This distance represents how much the classification represented by the point approaches the ideal situation, and the threshold that gives the point with the lowest distance constitutes the best one, in terms of compromise between specificity and sensibility (see Figure 4.3).

4.2 The ROC analysis applied to the image filtering

In the image filtering, the cut-off value is a gray level between 0 and 1 and, depending on its value, on the classified image there will be more or less white zones that correspond to the features identified by the filter. Changing

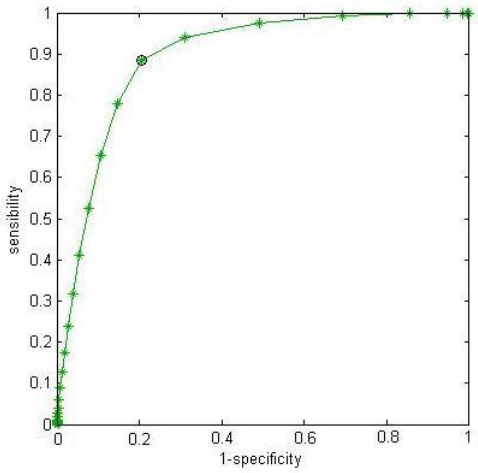

FIGURE 4.3: A ROC curve with the various points marked with a '*' and the best one evidenced with a circle.

the gray level cut-off value there will be more or less white areas because it changes the threshold that identifies the positives from the negatives (see Figure 4.4).

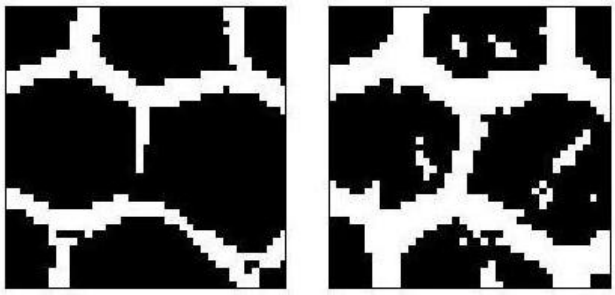

FIGURE 4.4: Crop of a same classified image but with two different gray level cut-off value. On the left with a cut of value of 0.2, on the right with a cut-off value of 0.3.

Each filtered image has been classified using 50 thresholds uniformly distributed from 0 to 1 (the distance between every two consecutive threshold is $1/50 = 0.02$) as described in Section 3.2 and each classified image has been compared with the *ground truth* image.

Minding that both the ground truth and the classified image have the *positives* (real and true respectively) marked with white pixels (gray level = 1), the number of true positive *TP*, true negative *TN*, false positive *FP* and false negative *FN* has been obtained first producing an image with the informations for every of the four categories:

- The *true positive* image has been obtained multiplying the *ground truth*

with the classified image. In the product image are left white only those pixels that are white in the classified images **and** in the *ground truth*, then the true positives;

- The *true negative* image has been obtained multiplying the negative of the *ground truth* image (that has in white the true negative) with the negative of the classified image (then marking in white the negative classified);

- The *false positive* image has been obtained subtracting the true positive image from the classified one. In this way to the classified image are subtracted all the true positives, leaving in white the false positives pixels;

- The *false negative* image has been obtained subtracting the true positive image from the *ground truth*. In this are left in white any pixel that is positive (white in the ground truth) but has been classified as negative (0 in the true positive image), constituting a false negative.

Then in each of these four images the white pixels has been counted to obtain the respective number of true and false positives/negatives.

For every threshold value, the number of *TP, TN, FP, FN* allows to calculate the specificity and sensitivity pair, to make the ROC curve. From the ROC curve the best cut-off value for that image is obtained with the method described on the previous section.

The data set in which the analysis has been performed consists on 30 images of the corneal endothelium, all of the same dimension but different for magnification, contrast, brightness and quality. In the tables below are reported the values of accuracy, sensitivity, specificity and AUC for every of the 30 images, in correspondence of the best thresholds listed on the last column.

4.2.1 Results on the filtering to detect the cells' edges

TABLE 4.1: Parameters resulting from the application of the filter for the edges detection, for every image, in correspondence of the best cut-off value.

Image num.	Accuracy	Sensitivity	Specificity	AUC	Best threshold
1	0.7174	0.7170	0.7175	0.7778	0.14
2	0.7328	0.7485	0.7293	0.8048	0.16
3	0.7338	0.7852	0.7227	0.8132	0.18
4	0.7494	0.7720	0.7446	0.8192	0.22
5	0.7143	0.7856	0.6989	0.8014	0.30
6	0.6723	0.7384	0.6583	0.7527	0.38
7	0.7190	0.7381	0.7149	0.7909	0.18
8	0.6923	0.8560	0.6568	0.8163	0.12
9	0.7573	0.7022	0.7698	0.7945	0.10
10	0.7301	0.7958	0.7156	0.8122	0.14
11	0.6996	0.7265	0.6936	0.7721	0.20
12	0.6793	0.7985	0.6535	0.7811	0.14
13	0.7984	0.7813	0.8013	0.8547	0.22
14	0.7067	0.7301	0.7016	0.7725	0.16
15	0.7309	0.7930	0.7179	0.8198	0.14
16	0.7142	0.6187	0.7270	0.7238	0.24
17	0.7146	0.8053	0.6932	0.8071	0.18
18	0.7195	0.7291	0.7175	0.7823	0.16
19	0.7754	0.8235	0.7664	0.8603	0.26
20	0.7829	0.6733	0.7972	0.7926	0.16
21	0.7243	0.7524	0.7184	0.7995	0.16
22	0.6604	0.7849	0.6326	0.7695	0.18
23	0.7509	0.7131	0.7594	0.7965	0.14
24	0.7457	0.7839	0.7375	0.8227	0.18
25	0.7100	0.7408	0.7033	0.7794	0.16
26	0.7627	0.6776	0.7814	0.7984	0.16
27	0.6918	0.8058	0.6680	0.7958	0.18
28	0.7427	0.8345	0.7243	0.8378	0.20
29	0.7451	0.6838	0.7586	0.7720	0.14
30	0.7065	0.7727	0.6924	0.7921	0.26

Mean values:	accuracy	0.7260	sensitivity	0.7556
	specificity	0.7191	AUC	0.7971
	best threshold	0.18		

4.2.2 Results on the filtering to detect the cells' trifurcations

TABLE 4.2: Parameters resulting from the application of the filter for the trifurcations detection, for every image, in correspondence of the best cut-off value.

Image num.	Accuracy	Sensitivity	Specificity	AUC	Best threshold
1	0.7431	0.8029	0.7373	0.8569	0.40
2	0.7799	0.8063	0.7779	0.8746	0.42
3	0.7719	0.8038	0.7694	0.8756	0.46
4	0.8037	0.7948	0.8044	0.8894	0.44
5	0.7691	0.7884	0.7675	0.8691	0.44
6	0.7379	0.7846	0.7349	0.8364	0.52
7	0.7745	0.7760	0.7743	0.8628	0.48
8	0.8007	0.7905	0.8016	0.8829	0.48
9	0.6763	0.8900	0.6581	0.8611	0.44
10	0.7878	0.8137	0.7858	0.8868	0.46
11	0.7586	0.7642	0.7582	0.8485	0.44
12	0.7334	0.8200	0.7250	0.8627	0.50
13	0.7671	0.8676	0.7645	0.9008	0.44
14	0.7410	0.8022	0.7350	0.8550	0.42
15	0.7741	0.8032	0.7723	0.8673	0.44
16	0.7473	0.7749	0.7469	0.8338	0.44
17	0.7679	0.7983	0.7648	0.8710	0.48
18	0.7757	0.7512	0.7771	0.8508	0.42
19	0.8086	0.8123	0.8085	0.8873	0.42
20	0.7341	0.8672	0.7327	0.8566	0.34
21	0.8029	0.7789	0.8045	0.8749	0.44
22	0.7437	0.7895	0.7389	0.8496	0.38
23	0.7662	0.8046	0.7636	0.8679	0.48
24	0.7810	0.8356	0.7767	0.8917	0.42
25	0.7858	0.7655	0.7876	0.8631	0.44
26	0.7963	0.7648	0.7990	0.8653	0.50
27	0.7956	0.7593	0.7982	0.8677	0.42

Continues on the next page

Continues from the previous page

Image num.	Accuracy	Sensitivity	Specificity	AUC	Best threshold
28	0.7901	0.8107	0.7889	0.8913	0.42
29	0.6519	0.8916	0.6309	0.8415	0.44
30	0.7836	0.7936	0.7829	0.8738	0.42

Mean values:	accuracy	0.7650	sensitivity	0.8035
	specificity	0.7622	AUC	0.8672
	best threshold	0.44		

4.2.3 Results on the filtering to detect the cells' centers

TABLE 4.3: Parameters resulting from the application of the filter for the centers detection, for every image, in correspondence of the best cut-off value.

Image num.	Accuracy	Sensitivity	Specificity	AUC	Best threshold
1	0.8143	0.8274	0.8083	0.8850	0.48
2	0.8341	0.8503	0.8248	0.9036	0.34
3	0.8336	0.8763	0.8091	0.9044	0.42
4	0.8507	0.8784	0.8350	0.9189	0.48
5	0.8364	0.8532	0.8272	0.9018	0.42
6	0.7923	0.8602	0.7467	0.8649	0.22
7	0.8011	0.8506	0.7757	0.8767	0.44
8	0.8344	0.9079	0.7962	0.9139	0.34
9	0.8346	0.8100	0.8474	0.8947	0.24
10	0.8357	0.8491	0.8282	0.9017	0.48
11	0.8153	0.8313	0.8073	0.8818	0.40
12	0.8266	0.8383	0.8212	0.8954	0.42
13	0.8467	0.8841	0.7960	0.8928	0.40
14	0.8075	0.8077	0.8075	0.8740	0.54
15	0.8403	0.8566	0.8289	0.8993	0.38
16	0.7038	0.7016	0.7080	0.7617	0.40
17	0.8334	0.8687	0.8183	0.9035	0.46
18	0.7871	0.7724	0.7980	0.8483	0.42
19	0.7998	0.7929	0.8075	0.8532	0.22

Continues on the next page

Continues from the previous page

Image num.	Accuracy	Sensitivity	Specificity	AUC	Best threshold
20	0.8173	0.8149	0.8226	0.8658	0.28
21	0.8255	0.8510	0.8089	0.8947	0.52
22	0.8133	0.8347	0.8044	0.8801	0.48
23	0.7948	0.8410	0.7662	0.8670	0.36
24	0.8368	0.8905	0.8062	0.9126	0.38
25	0.8020	0.8225	0.7918	0.8707	0.50
26	0.8033	0.8751	0.7653	0.8852	0.38
27	0.8179	0.8202	0.8165	0.8814	0.42
28	0.8590	0.8825	0.8409	0.9154	0.36
29	0.8052	0.8819	0.7662	0.8855	0.16
30	0.8040	0.7937	0.8101	0.8656	0.48

Mean values:	accuracy	0.8169	sensitivity	0.8408
	specificity	0.8030	AUC	0.8833
	best threshold	0.39		

4.3 Classification of a generic image

The last step of this analysis is to find which threshold to apply to a corneal endothelial image on a generic analysis. On a real application of this method no hand-made images are available: in fact, these images constitutes an ideal results of filtering and classification. Performing a manual segmentation, then, would make unnecessary the filtering. But the objective is to automate the segmentation: so, it's necessary to chose a gray level cut-off value to make the classification of a generic image.

From the filtering and the classification results on the thirty images set the goal is to chose a gray level cut off value to apply on any other image of the endothelium. To perform this analysis, four approaches are possible:

1. Make classification, comparison and ROC analysis applying to all the thirty images the mean value of the best threshold for every image;

2. Calculate the mean of the best thresholds for all the image except one, and using the mean value to make the classification to the excluded image; this procedure has to be repeated a number of times equal to the number of images, excluding each time a different image;

3. Apply the best threshold of an image to all the other images, for every image of the set;

4. Divide the image set into two parts, calculating the mean of the best thresholds for a half and applying the mean value to the other half set of images. Then repeat the same procedure with the two half reversed.

In this work the first approach has been chosen; the other three methods give a precision level that is unnecessary for this typology of analysis. The mean value of the best threshold is then the gray level cut-off value chosen to be "the most suitable" for a generic use on generic endothelial images.

To test this approach, the mean value of the best thresholds for every filtering operation on the entire image set (reported below each table in the previous section) is applied to classify again each image. The procedure is the same adopted to perform the classification with various thresholds values: the classified image is compared with the correspondent ground truth, allowing to calculate the sensitivity, specificity and accuracy values. Each sensitivity-specificity pair is plotted on a ROC space. In terms of best compromise between specificity and sensitivity, the image that has given the best performance is the one whose point in the ROC space approaches the upper left corner point (0,1).

It's important to denote that in this phase *no* ROC analysis is performed. The ROC analysis described on the previous section had the purpose of evaluating the best cut-off value on a classification for *one* image at time. Instead, in this case the test does not consist on finding the best cut-off values but only in applying a *unique* cut-off value for all the set of images and using the ROC space as a mean to find the best image with a technique similar to the one described on the previous section.

The tables on the following pages shows the accuracy, sensitivity and specificity values resulting from the classification of the filtered images with the mean value of the best thresholds of every image for each of the three filter typologies. It's interesting to denote the most suitable image, in terms of best compromise between sensibility and specificity: this image is highlighted in bold and reported on the page after each table.

4.3.1 Generic classification for the edge detection

Mean of the best thresholds: 0.18

TABLE 4.4: Results of the classification made with the mean value of the best thresholds for the edges detection.

Image num.	Accuracy	Sensitivity	Specificity
1	0.8022	0.4125	0.8887
2	0.7869	0.5952	0.8287
3	0.7445	0.7655	0.7399
4	0.6732	0.8709	0.6307
5	0.3377	0.9752	0.1998
6	0.1758	0.9999	0.0007
7	0.7308	0.7148	0.7343
8	0.8313	0.2267	0.9624
9	0.8154	0.0020	0.9998
10	0.7988	0.5365	0.8563
11	0.6645	0.7943	0.6354
12	0.7931	0.4284	0.8721
13	0.6902	0.8719	0.6596
14	0.7586	0.5881	0.7959
15	0.8187	0.5346	0.8782
16	0.4019	0.8678	0.3393
17	0.7278	0.7889	0.7134
18	0.7734	0.6031	0.8085
19	0.5079	0.9495	0.4256
20	0.8373	0.5613	0.8732
21	0.7755	0.6038	0.8117
22	0.6710	0.7631	0.6504
23	0.8220	0.3226	0.9341
24	0.7551	0.7600	0.7541
25	0.7647	0.5979	0.8012
26	0.8122	0.4259	0.8973
27	0.7078	0.7858	0.6915
28	**0.7014**	**0.8778**	**0.6661**
29	0.8215	0.0532	0.9906
30	0.4787	0.9403	0.3806

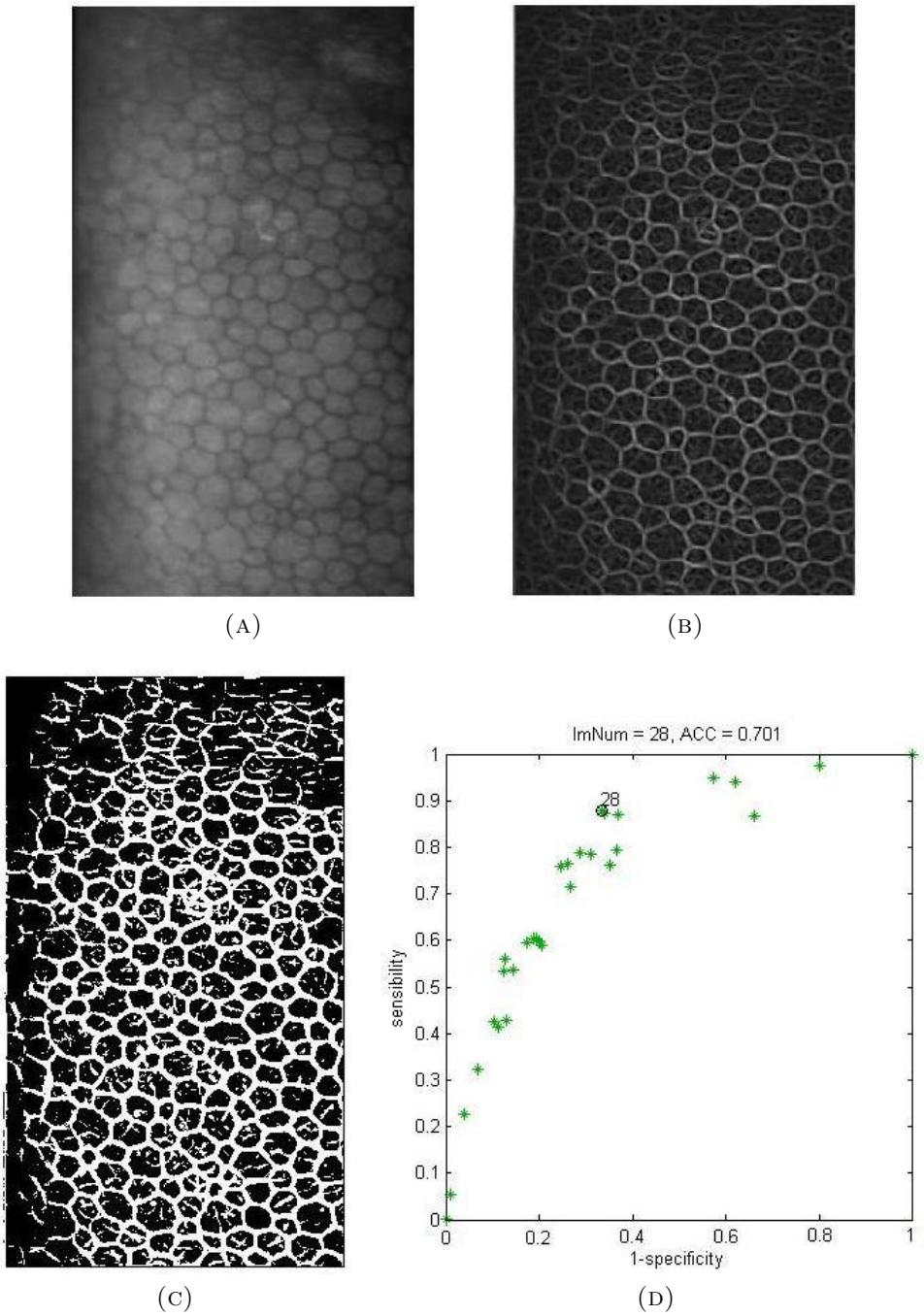

(A) (B)

(C) (D)

FIGURE 4.5: The image number 28 has resulted the most suitable for the edge filter. The figures above shows the original image (A), the image filtered (B), the classified image with the mean of the best thresholds (C) and the points in the ROC space with the one corresponding to image 28 evidenced.

4.3.2 Generic classification for the trifurcations detection

Mean of the best thresholds: 0.44

TABLE 4.5: Results of the classification made with the mean value of the best thresholds for the trifurcations detection.

Image num.	Accuracy	Sensitivity	Specificity
1	0.8645	0.6099	0.8891
2	0.8374	0.6989	0.8480
3	0.7187	0.8638	0.7075
4	0.8078	0.7894	0.8093
5	0.7725	0.7858	0.7714
6	0.4076	0.9726	0.3718
7	0.6467	0.8983	0.6246
8	0.5315	0.9700	0.4939
9	0.6918	0.8793	0.6758
10	0.7344	0.8657	0.7242
11	0.7634	0.7579	0.7639
12	0.3883	0.9881	0.3304
13	**0.7711**	**0.8619**	**0.7688**
14	0.8164	0.6962	0.8280
15	0.7799	0.7959	0.7789
16	0.7547	0.7679	0.7545
17	0.5904	0.9397	0.5549
18	0.8468	0.6389	0.8587
19	0.9269	0.5908	0.9379
20	0.9637	0.2957	0.9705
21	0.8064	0.7748	0.8086
22	0.8857	0.4659	0.9299
23	0.5549	0.9380	0.5289
24	0.8479	0.7369	0.8566
25	0.7900	0.7583	0.7928
26	0.3380	0.9917	0.2831
27	0.8516	0.6640	0.8651
28	0.8477	0.7349	0.8540
29	0.6702	0.8764	0.6521
30	0.8422	0.7107	0.8524

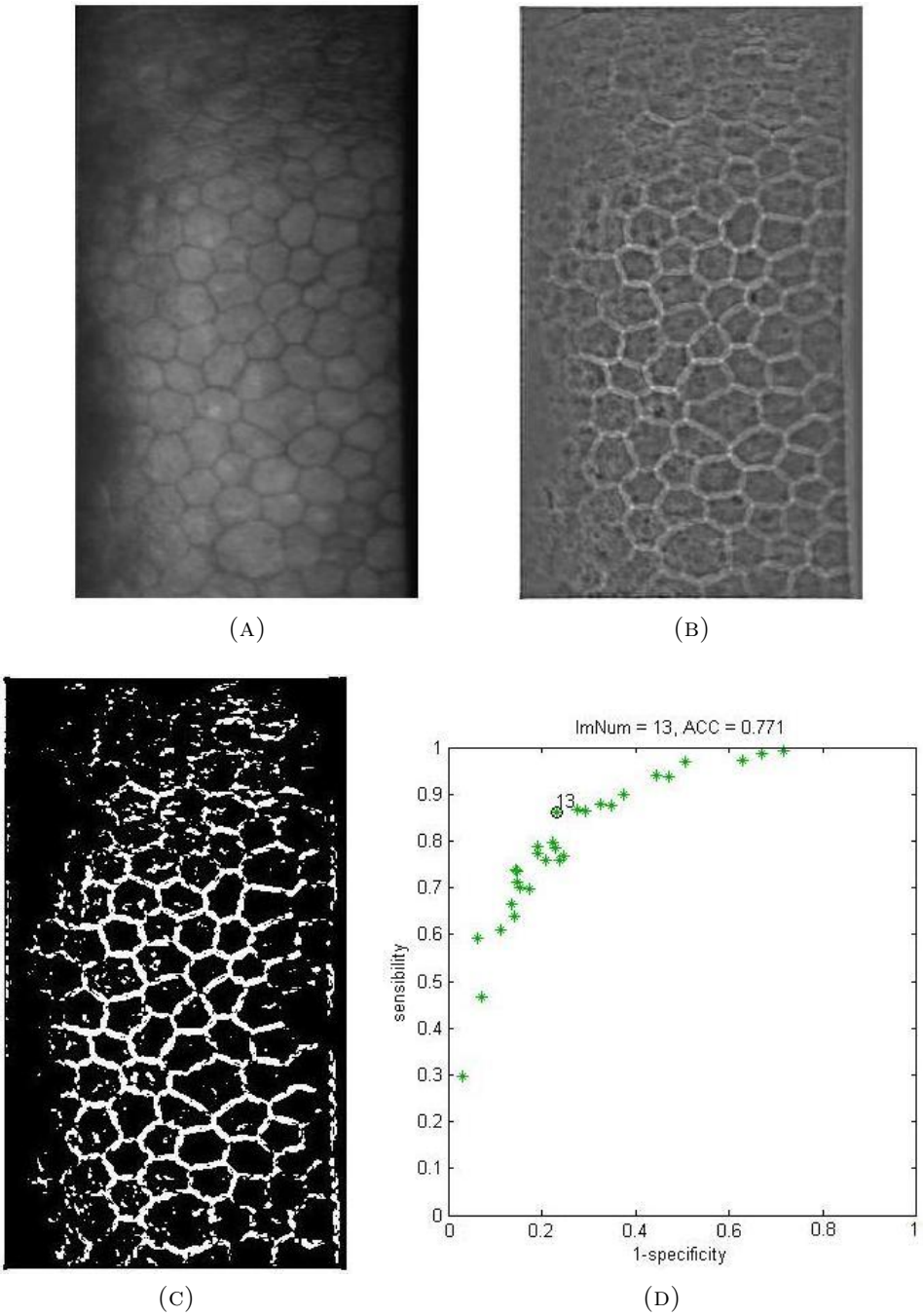

(A) (B)

(C) (D)

FIGURE 4.6: The image number 13 has resulted the most suitable for the trifurcation filter. The figures above shows the original image (A), the image filtered (B), the classified image with the mean of the best thresholds (C) and the points in the ROC space with the one corresponding to image 13 evidenced.

4.3.3 Generic classification for the centers detection

Mean of the best thresholds: 0.39

TABLE 4.6: Results of the classification made with the mean value of the best thresholds for the centers detection.

Image num.	Accuracy	Sensitivity	Specificity
1	0.4497	0.9927	0.2040
2	0.8176	0.6299	0.9262
3	0.7989	0.9283	0.7247
4	0.6013	0.9897	0.3812
5	0.8034	0.9185	0.7401
6	0.6392	0.1199	0.9875
7	0.6762	0.9475	0.5367
8	0.8368	0.6776	0.9197
9	0.6626	0.0182	0.9994
10	0.6212	0.9790	0.4192
11	0.8103	0.8484	0.7913
12	0.7970	0.8981	0.7506
13	0.8488	0.9059	0.7715
14	0.3266	1.0000	0.0075
15	0.8377	0.8016	0.8630
16	0.7194	0.7382	0.6815
17	0.6659	0.9638	0.5384
18	0.7665	0.8605	0.6963
19	0.4722	0.0016	1.0000
20	0.4236	0.1853	0.9708
21	0.4268	0.9994	0.0554
22	0.4770	0.9816	0.2654
23	0.8017	0.7157	0.8549
24	**0.8448**	**0.8541**	**0.8395**
25	0.3861	0.9961	0.0827
26	0.8203	0.8250	0.8178
27	0.7998	0.8885	0.7446
28	0.8341	0.7515	0.8977
29	0.6628	0.0000	1.0000
30	0.5720	0.9670	0.3407

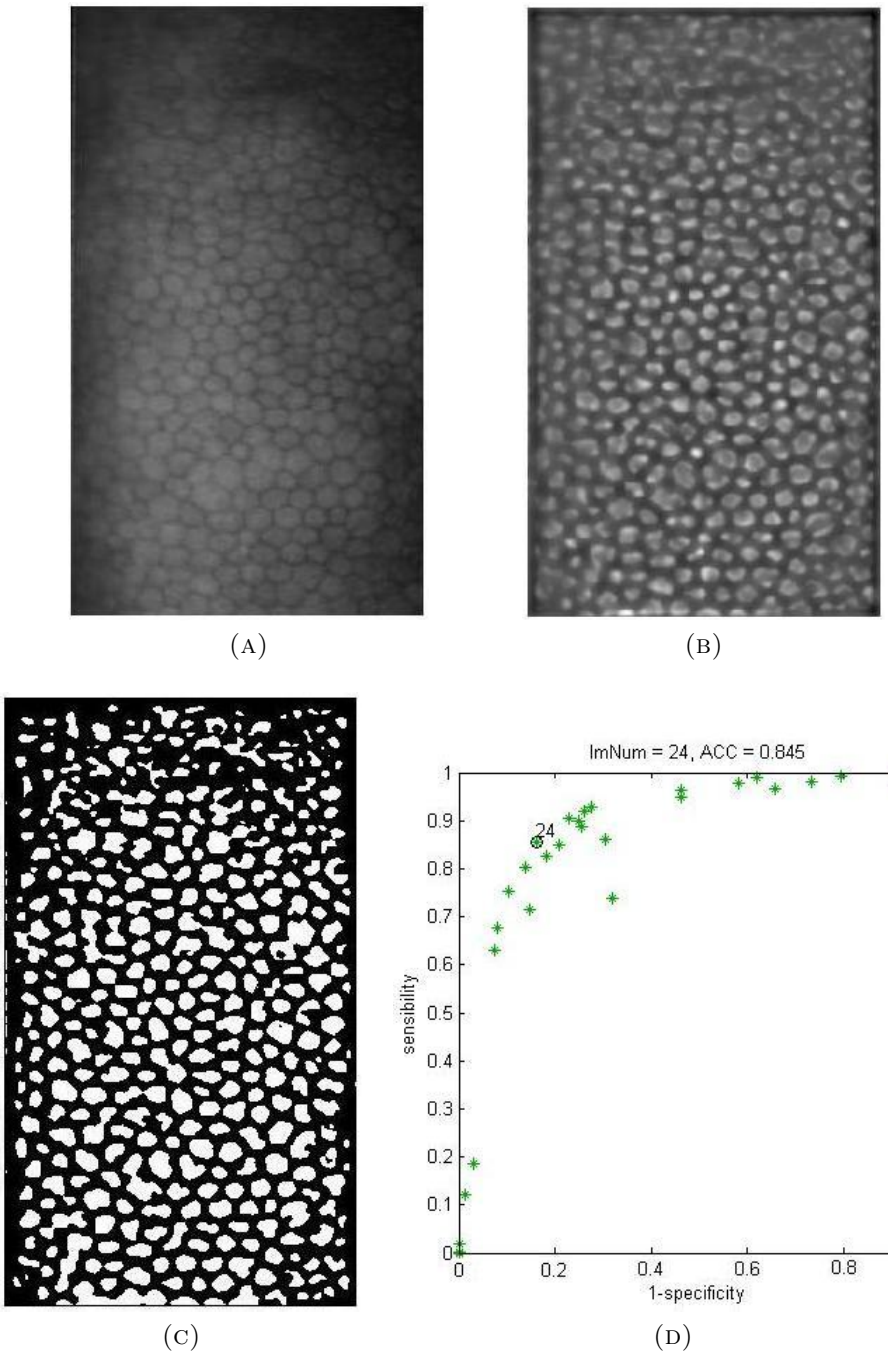

(A) (B)

(C) (D)

FIGURE 4.7: The image number 24 has resulted the most suitable for the centers filter. The figures above shows the original image (A), the image filtered (B), the filtered image classified with the mean of the best thresholds (C) and the points in the ROC space with the one corresponding to image 24 evidenced.

Chapter 5

Conclusions

The corneal endothelium images analysis is an important study to achieve information regarding the health state of the cornea. This work had the objective not to develop a method to achieve the parameters that are clinically relevant to determine an eventual corneal disease but to verify if the filtering in the spatial domain and the sequent classification are good instruments to achieve informations on the corneal endothelial images about the cellular borders; informations that on a following step could be used to evaluate the parameters described on Chapter 1.

The filtering operations have been conducted without having any standards to construct the three types of filters. The features that had to be detected (cells' edges, centers and trifurcations) are present on the original images with different characteristics in terms of length, thickness, areas and angles of orientation. This makes impossible to know *a priori* the characteristics that the filter could have to be optimal. The construction of the filters have been made simply trying different values of scales, chosen reasonably, and bringing the one that gives the best result.

The set of thirty images on which the filtering and the sequent analysis has been performed was not of the best quality for the detections of borders, due to the lower definition that gives blurred contours. This is a lack of the image system of acquisition that cannot be repaired with an algorithm of pre-elaboration of the images; that is, it's impossible to achieve informations from an image that has not.

The usage of a ground truth allows to isolate regions in which good informations can be achieved. The characteristics of the used ground truth can influence the results: for example changing the cells' edges thickness on the correspondent ground truth changes the number of positives and negatives and, without changing the the corresponding filter's dimensions, the analysis results will change. It would be a solution finding a method that joins the

characteristics of the features in the ground truth with the parameters that characterize the filter. However, the purpose of this analysis is to find features with a good precision on *where* it's located and not *how* it's made. It's then important to use a ground truth that gives correct informations on the positions of the features rather than their dimensions, but without exceeding in them, in order to not identify a priori positives or negatives pixels that in the original image never could be.

With the ground truth and the filters described, the results regarding the ROC analysis have been quite good, with a global accuracy, sensitivity and specificity values between the 71% and the 84%. In particular, the filter to detect the cells' centers has been the one with the best performance. This is probably due to the fact that the cells' centers are the features that are less difficult to detect on the corneal endothelium images, because they occupy areas that have about the same shape, rather than an edge or a trifurcation that have more variability on their characteristics.

The image that results the most suitable for each filtering operation has been chosen with the same approach used for the research of the best gray level cut-off value: the one that gives the best compromise between sensitivity and specificity. The three cases have given three different most suitable images. This suggest that in the set of 30 images there are not "better" or "worse" images, but images that results more suitable for some reasons that cannot be identify with precision (for example for a better contrast, brightness or other factors). For this reason, performing the filtering and the analysis on a set of image and then the research of the most suitable one is a good technique in order to give to eventual following studies an image that contains the best informations content.

Bibliography

[1] C. Murphy, J. Alvarado, R. Juster, M. Maglio, *Prenatal and postnatal cellularity of the human corneal endothelium. A quantitative histologic study.* Investigative Ophthalmology & Visual Science, vol. 25, no. 3, pages 312-322, March 1984.

[2] Gary S.L. Peh, Roger W. Beuerman, Alan Colman, Donald T. Tan, Jodhbir S. Mehta, *Human Corneal Endothelial Cell Expansion for Corneal Endothelium Transplantation: An Overview*, Transplantation, vol. 91, pages 811-819, 27 April 2011.

[3] Bernard E. McCarey, Henry F. Edelhauser, Michael J. Lynn, *Review of Corneal Endothelial Specular Microscopy for FDA Clinical Trials of Refractive Procedures, Surgical Devices and New Intraocular Drugs and Solutions*. Cornea. 27(1), pages 1-16, January 2008. Available on PubMed Central.

[4] A. Lucente, *L'endotelio nell'imaging corneale*, Oftalmologia domani, no. 2, 2011.

[5] M. R. Azimi, *Digital Image Processing, Lecture 19 & 20*, Department of Electrical and Computer Engineering, Colorado State University, spring 2013.

[6] Rafael C. Gonzales, Richard E. Woods, *Digital Image Processing*, 2nd edition, Upper Saddle River, N.J.: Prentice Hall, 2002.

[7] Ezio Bottarelli, Stefano Parodi, *Un approccio per la valutazione della validitá dei test diagnostici: le curve R.O.C. (Receiver Operating Characteristic)*. Annuario della Facoltá di Medicina Veterinaria, Universitá di Parma, vol. 23, pages 49-68, 2003.

[8] Tom Fawcett, *An introduction to ROC Analysis*, Pattern recognition letters 27.8: pages 861-874, 2006.